

Droplet–String Deformation and Stability during Microconfined Shear Flow

Jai A. Pathak* and Kalman B. Migler*

National Institute of Standards and Technology, Polymers Division, 100 Bureau Drive,
Gaithersburg, Maryland 20899-8544

Received April 23, 2003. In Final Form: July 24, 2003

We have performed experiments on model emulsions of polyisobutylene (PIB) and poly(dimethylsiloxane) (PDMS) to quantify the effect of confinement on deformation and stability under flow of droplets and strings (threads). It is known from earlier work from our group that, under confinement, droplets in concentrated emulsions can coalesce with each other and elongate in the flow direction to form stable strings. In the present context, strings can be simply viewed as droplets having a large aspect ratio whereas, in the bulk case, there are two known states of a droplet (stable and unstable), as determined by the droplet Capillary number (Ca). We find that confinement effects induce three additional states: squashed drops, stable strings, and unstable strings. For strings, deformation under confinement is a very strong function of Ca : the aspect ratio of a string scales nearly as Ca^3 . This scaling relationship is *unique* to confinement, and it sets strings apart from transiently stretched droplets in the bulk. Confinement not only promotes deformation but also allows larger stable droplets to exist under flow than what is predicted by the critical Ca . Strings are stabilized by a combination of the shear flow field and wall effects arising from confinement.

Introduction

Since the pioneering work of Geoffrey Taylor^{1,2} on the formation of emulsions in simple shear and hyperbolic flow fields, much effort has been directed at the study of drop deformation and breakup in emulsions in various different kinds of flow fields. Several excellent reviews are available which survey this field at different stages of its development.^{3–11} When an emulsion is deformed in a shear flow field, interfacial tension tends to restore the emulsion droplets to spherical shape (in the presence of finite size effects, this spherical structure can be distorted), while shear stress tends to perturb the droplets from the spherical state. Droplets deform until the interfacial tension effects can no longer balance the shear stress induced deformation, at which point they break up. These competing effects are parametrized by the ratio of viscous and equilibrium interfacial stresses of a spherical droplet in the dimensionless Capillary number, Ca .

$$Ca = \frac{\eta_m \dot{\gamma} R}{\sigma} \quad (1)$$

Here η_m , $\dot{\gamma}$, R , and σ denote matrix viscosity, shear rate, drop radius, and interfacial tension, respectively. Taylor quantified deformation of a droplet with major and minor

axes a and b , respectively, in terms of the deformation parameter D .

$$D = \frac{a - b}{a + b} \quad (2)$$

Following Bentley and Leal,¹² we quantify deformation here in terms of the aspect ratio, $D' = a/b$, which is more appropriate for highly elongated objects with large aspect ratios. Of course, D' and D are easily related to each other.

$$D' = \frac{1 + D}{1 - D} \quad (3)$$

Note that the object whose deformation is being quantified in this work can be either a droplet or a string. Taylor's *single-droplet* theory predicts a linear dependence of D on Ca for small deformation. We emphasize the fact that Taylor analysis assumes infinitesimal deformation, and any application to large deformations is inappropriate.

$$D = CaF(p); \quad F(p) = \frac{19p + 16}{16p + 16}$$

$$D' = \frac{1 + CaF(p)}{1 - CaF(p)} \quad (4)$$

When Ca exceeds a critical value, which depends on the viscosity ratio $p = \eta_d/\eta_m$ (η_d is the droplet viscosity), the droplets become unstable, and the corresponding Ca is known as the critical Capillary number, Ca_{cr} , which effectively sets a limiting size scale for the stability of a drop. If we denote this largest stable droplet size as R^* , then it follows from eq 1 that

$$Ca_{cr} = \frac{R^* \eta_m \dot{\gamma}}{\sigma} \quad (5)$$

which is trivially rearranged to explicitly write R^* .

* Corresponding authors. E-mail: Jai.Pathak@nist.gov; Kalman.Migler@nist.gov.

- (1) Taylor, G. I. *Proc. R. Soc. London, A* **1932**, *138*, 41–48.
- (2) Taylor, G. I. *Proc. R. Soc. London, A* **1934**, *146*, 501–523.
- (3) Acrivos, A. *Ann. N. Y. Acad. Sci.* **1983**, *404*, 1–11.
- (4) Rallison, J. M. *Annu. Rev. Fluid Mech.* **1984**, *16*, 45–66.
- (5) Grace, H. P. *Chem. Eng. Commun.* **1982**, *14*, 225–277.
- (6) Stone, H. A. *Annu. Rev. Fluid Mech.* **1994**, *26*, 65–102.
- (7) Tucker, C. L.; Moldenaers, P. *Annu. Rev. Fluid Mech.* **2002**, *34*, 177–210.
- (8) Briscoe, B. J.; Lawrence, C. J.; Mietus, W. G. P. *Adv. Colloid Interface Sci.* **1999**, *81*, 1–17.
- (9) Goldsmith, H. L.; Mason, S. G. *The Microrheology of Dispersions. In Rheology: Theory and Applications*; Eirich, F. R., Ed.; Academic Press: New York, 1967; Chapter 2, pp 85–250.
- (10) Leal, L. G. *Annu. Rev. Fluid Mech.* **1980**, *12*, 435–476.
- (11) Mason, T. G. *Curr. Opin. Colloid Interface Sci.* **1999**, *4*, 231–238.

- (12) Bentley, B. J.; Leal, L. G. *J. Fluid Mech.* **1986**, *167*, 241–283.

$$R^* = \frac{\sigma Ca_{cr}}{\eta_m \dot{\gamma}} \quad (6)$$

From single-droplet experiments, estimates of $Ca_{cr}(p)$ are available for various different flow fields, ranging from simple shear,¹³ which contains equal parts of stretching and solid-body rotation,¹⁴ to pure hyperbolic (only stretching and no rotational component), and other intermediate flow fields as well.^{12,15–17} For a system with a fixed value of p , Ca_{cr} is constant, which simply implies that $R^* \propto \dot{\gamma}^{-1}$. The simple implication of this idea is that the limiting droplet size (we take it to equal the Taylor prediction in this paper, for simplicity) evolves itself upon changing $\dot{\gamma}$, so as to correspond to criticality. We apply this idea in the experiments described in this paper to determine how this length scale compares with droplet size in concentrated emulsions under microscopic confinement.

The single-droplet case is the foundation for understanding the phenomenology underlying breakup, which is critical for the case of a concentrated emulsion or polymer blend. Recent measurements of droplet breakup in systems with nonvanishing concentrations¹⁸ have revealed, in agreement with our intuition, that the effective Ca_{cr} is smaller in a concentrated emulsion than that in a single-drop analogue of the same system, presumably due to droplet–droplet collisions which promote breakup. We do, however, also note that there are data in the literature that suggest that Ca_{cr} in a concentrated emulsion is larger than the single-drop analogue.¹⁹ Concentrated emulsions are, of course, characterized by simultaneous coalescence and breakup, whose interplay leads to a statistical distribution of R and consequently for Ca . Computational work by different groups has exploited numerical simulations to investigate the microstructure and rheology of concentrated systems,^{20–26} made possible by strides in computing capability in the past decade.

A common feature of most studies on emulsion rheology and morphology under flow is that they have all addressed the “bulk” regime, where the characteristic droplet size R is much smaller than the characteristic length scale between the confining surfaces, that is, the gap between parallel plates (d). Previous work from our group on confined poly(dimethylsiloxane) (PDMS)–polyisobutylene (PIB) emulsions has shown that finite size effects (realized when $2R \approx d$) can strongly influence droplet microstructure, causing formation of stable strings (threads)²⁷ and also resulting in droplet layering in the velocity gradient/flow plane.^{28,29} Similarly, Mietus et al.³⁰ have reported

finite-size effects in the Couette flow of water drops in oil in a horizontal annular cell; the manifestations of finite size effects include formation of toroidal rings and water sheaths. A very important difference between their oil–water experimental system and our system is that the Bond number $Bo = \Delta\rho g R^2 / \sigma$ ($\Delta\rho$ is the difference between component densities, and g is the acceleration due to gravity), which quantifies the ratio of hydrostatic pressure to interfacial tension effects, is approximately 7.5 for their system, while in our PDMS–PIB system $Bo \approx 10^{-4}$. This signifies that buoyancy dominates over interfacial tension effects in their system, while the reverse holds true in our system. We focus on our system with small Bo ($\ll 1$).

For now, we offer an operational definition of a string: its width in the vorticity direction (b) is smaller than d , and it has an appreciably large aspect ratio ($a/b \geq 4$). Later in this paper, we will make this definition more comprehensive and quantitative. We must carefully distinguish between a string and a “ribbon”, even though they can have comparable aspect ratios; for ribbons, $b > d$ (which means that they are squashed by the platens), while, for strings, $b < d$.

In this work we address droplet/string deformation in confined concentrated emulsions in order to answer the following questions. How does confinement affect droplet deformation? What length scales are relevant in determining the microstructure under confinement? If we think of a string as an extension of a droplet, then we can also determine the size of the largest stable droplet that can survive during flow. We perform carefully designed experiments to answer these questions and show that droplet/string deformation behavior in microconfined emulsions reveals new regimes of deformation hitherto not seen in emulsions in the bulk.

As discussed above, in a concentrated emulsion, there is a statistical distribution of droplet sizes due to simultaneous breakup and coalescence. In the experiments and analysis below, we measure the aspect ratio of the droplets in this distribution as a function of droplet size. Thus, in one experiment, we can probe many droplet sizes at the same time. The deformation (aspect ratio) of a given droplet is unaffected by proximity to a neighboring droplet as long as the droplets are separated by a distance greater than their characteristic size. The emphasis of this work is thus on steady-state structures, and so we can use this experimental protocol to extract the single-droplet deformation behavior as a function of droplet size.

Experimental Section

PIB (mass average molecular mass, $M_w = 800$; PolySciences)⁵⁵ and PDMS ($M_w = 62\,700$; Gelest) samples used here have zero shear viscosities $\eta_0 = 10$ Pa·s at 25 °C,²⁸ yielding $p = 1$. The pure components, which have no measurable elasticity, behave as well-defined Newtonian liquids under these conditions. The density difference between PIB and PDMS is small, rendering gravitational effects negligible ($\rho_{PIB} = 890$ kg/m³ at 20 °C and $\rho_{PDMS} = 970$ kg/m³ at 20 °C;³¹ droplet to matrix density ratio, $\kappa = 1.08$). The value of σ for the PDMS/PIB system is 2.5 mN/m.³² An emulsion containing 9.7% mass fraction PDMS in the PDMS/PIB mixture was prepared and used in this study.

(29) Pathak, J. A.; Robertson, E.; Hudson, S. D.; Migler, K. B. Droplet Microstructure and String Stability in Sheared Emulsions: Role of Finite-Size Effects. In *Nonlinear Dynamics in Polymeric Systems*; Pojman, J., Tran-Cong, Q., Eds.; American Chemical Society: Washington, DC, 2003.

(30) Mietus, W. G. P.; Matar, O. K.; Seevaratnam, G.; Wong, A.; Briscoe, B. J.; Lawrence, C. J. *Phys. Rev. Lett.* **2001**, *86*, 1211–1214.

(31) Minale, M.; Moldenaers, P.; Mewis, J. *Macromolecules* **1997**, *30*, 5470–5475.

(32) Wagner, M.; Wolf, B. A. *Macromolecules* **1993**, *26*, 6498–6502.

(13) Karam, H. J.; Bellinger, J. C. *Ind. Eng. Chem. Fundam.* **1968**, *7*, 576–581.

(14) Batchelor, G. K. *An Introduction to Fluid Dynamics*; Cambridge University Press: Cambridge, 1974.

(15) Stone, H. A.; Bentley, B. J.; Leal, L. G. *J. Fluid Mech.* **1986**, *173*, 131–158.

(16) Stone, H. A.; Leal, L. G. *J. Fluid Mech.* **1989**, *198*, 399–427.

(17) Stone, H. A.; Leal, L. G. *J. Fluid Mech.* **1989**, *206*, 223–263.

(18) Jansen, K. M. B.; Agterof, W. G. M.; Mellema, J. *J. Rheol.* **2001**, *45*, 227–236.

(19) Sundararaj, U.; Macosko, C. W. *Macromolecules* **1995**, *28*, 2647–2657.

(20) Li, X.; Charles, R.; Pozrikidis, C. *J. Fluid Mech.* **1996**, *320*, 395–416.

(21) Charles, R.; Pozrikidis, C. *J. Fluid Mech.* **1998**, *365*, 205–234.

(22) Kennedy, M. R.; Pozrikidis, C.; Skalak, R. *Comput. Fluids* **1994**, *23*, 251–278.

(23) Zhou, H.; Pozrikidis, C. *Phys. Fluids A* **1993**, *5*, 311–324.

(24) Loewenberg, M.; Hinch, E. J. *J. Fluid Mech.* **1996**, *321*, 395–419.

(25) Zinchenko, A. Z.; Davis, R. H. *J. Fluid Mech.* **2002**, *455*, 21–62.

(26) Loewenberg, M. *J. Fluids Eng.* **1998**, *4*, 824–832.

(27) Migler, K. B. *Phys. Rev. Lett.* **2001**, *86*, 1023–1026.

(28) Pathak, J. A.; Davis, M. C.; Hudson, S. D.; Migler, K. B. *J. Colloid Interface Sci.* **2002**, *255*, 391–402.

All flow visualization experiments were performed in a Linkam CSS-450 commercial shear cell with parallel quartz platens (see ref 28 for a detailed description). The gap between the parallel plates was set to $36 \pm 3 \mu\text{m}$. The estimate of the standard uncertainty in the gap was made optically, as we verified the gap width between the plates by measuring the translation of the microscope stage between focusing on a scratch on the top plate and a scratch on the bottom plate. When air is present between the plates, this translation gives the gap width, while when the emulsion is present between the plates, this translation must be multiplied by an average refractive index for the emulsion (taken to be 1.5) to determine the actual gap width. The shear cell (interfaced with a PC to control gap width, shear rate, and temperature) is placed on the stage of an optical microscope (Carl Zeiss). Objectives of $3.5\times$, $10\times$, $20\times$, and $40\times$ magnification were used at each shear rate (except at the shear rate $\dot{\gamma} = 3.0 \text{ s}^{-1}$, where only $3.5\times$ magnification was used, to concentrate on the string and squashed droplet morphology). Images were acquired with an analog video camera (Pulnix TM-9701), and frames were grabbed by means of a Labview IMAQ PCI/PXI-1409 image acquisition board. Lengths were quantified on National Instruments IMAQ Vision Builder Software (v. 5.0).

Experiments were performed at $25 \pm 1 \text{ }^\circ\text{C}$. The Reynolds number $Re = \rho\dot{\gamma}R_0^2/\eta_m \sim O(10^{-8})$ involved in these experiments is small, signifying Stokes flow (ρ denotes fluid density). The experimental procedure involved placing the emulsion sample between the plates (after gentle stirring) and then setting the gap (which was verified with the sample present between the plates). The system was first presheared (at the beginning of the experiment only) at $\dot{\gamma} = 10 \text{ s}^{-1}$ for 20 min to generate a tight droplet size distribution with a small polydispersity. At 10 s^{-1} , fine droplets are produced, from which subsequent microstructures are generated by the interplay of breakup and coalescence. The experiment was then started by shearing the mixture at $\dot{\gamma} = 0.75 \text{ s}^{-1}$ for 3 h, and then data were acquired by grabbing frames. Video data of the emulsion under flow were also saved on S-VHS videotape. After that, the shear rate was increased to $\dot{\gamma} = 1.75 \text{ s}^{-1}$, and data were acquired at this shear rate as described earlier. The system was taken directly from one shear rate to the next higher shear rate. In this way, data were also acquired at $\dot{\gamma} = 2.5, 3.0, 4.0, 5.25, 6.5, 7.5, 8.5, \text{ and } 10 \text{ s}^{-1}$. For the sake of brevity, we only discuss detailed results at some particular shear rates (see next section), which are representative of all the microstructural states sampled in these experiments.

Analysis of the collected data involved the determination of the aspect ratio D and Ca of the droplets and strings. To cast the dependence of D in terms of Ca , it was necessary to determine the radius, R_0 , of the equivalent spherical droplet. As we observe in the flow-vorticity plane, we must compute the shape and thickness of the droplets in the flow-gradient direction. R_0 was easily determined for strings ($D \geq 4$) by equating the volume of the cylindrical string ($\pi ab^2/4$) to that of the equivalent sphere ($4\pi R_0^3/3$) and ignoring the negligibly small contribution from the string ends. In the “small droplet” case ($R_0 < d$), the relaxed state of the droplet (seen upon cessation of flow) is a reliable indicator of its quiescent radius. To determine R_0 , flow was stopped temporarily to allow these small droplets to relax back to spheres. This posed a problem at those shear rates where droplets and strings coexist (e.g., at $\dot{\gamma} = 3.0 \text{ s}^{-1}$), as the strings start to break up upon cessation of shear. To circumvent this problem, flow was stopped only at the very end of measurements at that shear rate, just before stepping up to the next higher shear rate (e.g., stepping from $\dot{\gamma} = 3.0 \text{ s}^{-1}$ to $\dot{\gamma} = 4.0 \text{ s}^{-1}$). However, when $R_0 > d$, finite-size effects deform the droplet, and its observed radius R is certainly larger than R_0 . In this case, an assumption is needed about the three-dimensional shape of deformed droplets; it is assumed that, under flow, a squashed droplet is an ellipsoid whose height (c) in the gradient direction spans the entire gap width d , and therefore its volume under flow equals $4/3\pi(a/2)(b/2)(d/2)$. Upon equating this volume of the flowing ellipsoid to $4\pi R_0^3/3$, R_0 can be estimated for squashed droplets.

Experimental Results and Discussions

We first discuss representative data on the emulsion at $\dot{\gamma} = 0.75 \text{ s}^{-1}$ in Figures 1 and 2. In this work, we make the

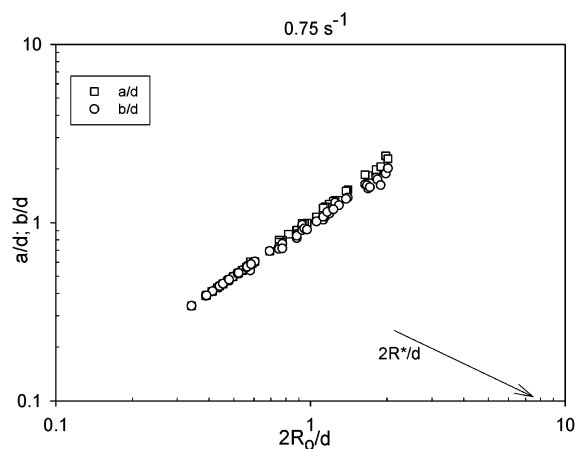


Figure 1. Droplet end-to-end length and dimension in the vorticity direction versus equivalent droplet diameter (all length scales have been rendered dimensionless by the gap width between parallel plates) at $\dot{\gamma} = 0.75 \text{ s}^{-1}$.

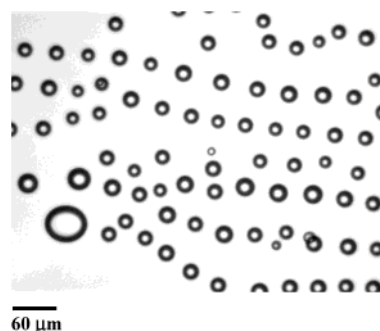


Figure 2. Optical micrograph of morphology at $\dot{\gamma} = 0.75 \text{ s}^{-1}$.

shear rate dimensionless by $\dot{\gamma}_d$, which is the Taylor estimate of the shear rate at which the droplet size is $O(d)$, defined by $(\eta_m \dot{\gamma}_d d / \sigma) = 1$. Using $d = 36 \mu\text{m}$, $\eta_m = 10 \text{ Pa}\cdot\text{s}$, and $\sigma = 2.5 \times 10^{-3} \text{ N/m}$, we get $\dot{\gamma}_d = 6.94 \text{ s}^{-1}$. Thus, at $\dot{\gamma} = 0.75 \text{ s}^{-1}$, we have $\dot{\gamma}/\dot{\gamma}_d = 0.108$. The measured values of a/d and b/d at this shear rate are plotted as a function of $2R_0/d$ in Figure 1. At this shear rate, droplets with size smaller and larger than the gap width are found (see Figure 2) and a/b values for the small and squashed droplets are rather small, $O(1)$, as Ca is ~ 0.1 , even for the larger drops. At this shear rate, a and b scale with R_0 with an exponent nearly equal to 1.

$$(a/d) \propto (R_0/d)^{1.07 \pm 0.04} \quad (7)$$

$$(b/d) \propto (R_0/d)^{0.95 \pm 0.02} \quad (8)$$

We shall soon see that the scaling exponents in the dependence of a and b on R_0 are appreciably different for the string morphology. At this shear rate $2R_0/d = 7.38$ is significantly greater than 1.

Upon increasing $\dot{\gamma}$ to 1.75 s^{-1} ($\dot{\gamma}/\dot{\gamma}_d = 0.252$), we see coexistence of three distinct morphological objects: drops, squashed droplets, and strings (see Figures 3 and 4). The appearance of strings in addition to droplets and squashed drops adds a branch to the a/b versus Ca curve. While there is definitely a distribution of string/ribbon widths, there is no dependence of the width on the total string/ribbon mass. For strings, the $2R_0/d$ considerably exceeds $2R_0/d$, pointing to the fact that strings form when the diameter of the equivalent sphere grows (through the equilibrium between statistical coalescence and breakup) large enough to allow the flow field to stretch the drop in

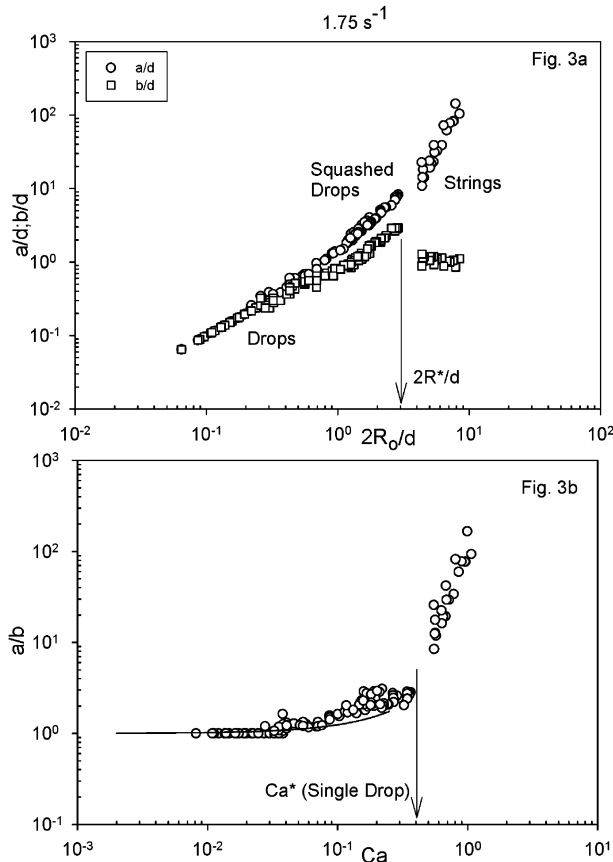


Figure 3. (a) Droplet end-to-end length and dimension in the vorticity direction versus equivalent droplet diameter (all length scales have been rendered dimensionless by the gap width between parallel plates) at $\dot{\gamma} = 1.75 \text{ s}^{-1}$. (b) Aspect ratio versus Capillary number at $\dot{\gamma} = 1.75 \text{ s}^{-1}$. The Taylor theory prediction for deformation is also shown as the smooth curve.

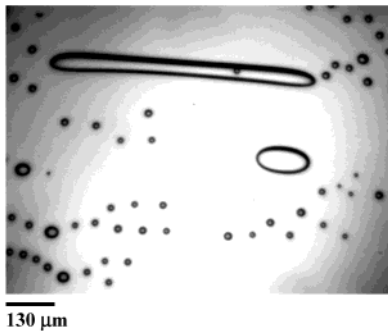


Figure 4. Optical micrograph of the morphology at $\dot{\gamma} = 1.75 \text{ s}^{-1}$.

the flow direction. The equivalent sphere for strings is supercritical, as their $Ca > Ca_{cr}$. Note that, at this shear rate, $2R^*/d (=3.16)$ has moved closer to 1, which means that the droplets have to attain a smaller size at $\dot{\gamma} = 1.75 \text{ s}^{-1}$ (compared to $\dot{\gamma} = 0.75 \text{ s}^{-1}$) in order to form strings. Squashed droplets are wider in the vorticity direction than strings, and this difference in b/d for them is reflected in both Figure 3 (notice the reduction in b/d in the transition from squashed droplets to strings) and also in Figure 4, where the squashed droplet is visibly wider than the string. The continuous curve in Figure 3b is the D prediction of the Taylor theory, eq 4. The deviation between experimental data and the theoretical prediction becomes obvious in the squashed droplet region. The prediction curve is not extended into the string region, as bulk isolated droplets are not stable for $Ca > Ca_{cr}$.

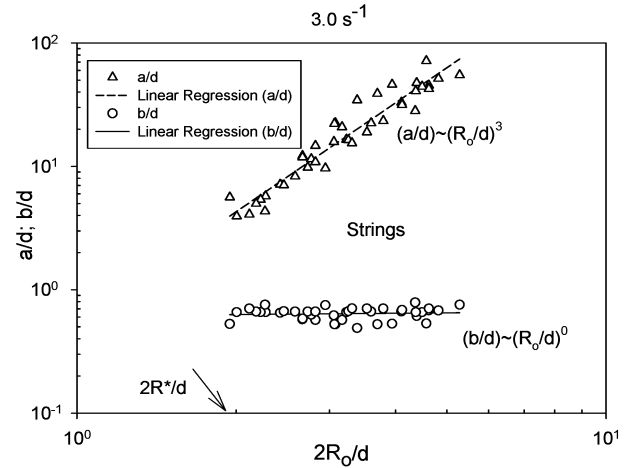


Figure 5. Droplet end-to-end length and dimension in the vorticity direction versus equivalent droplet diameter (all length scales have been rendered dimensionless by the gap width between parallel plates) at $\dot{\gamma} = 3.0 \text{ s}^{-1}$, for the string morphology only.

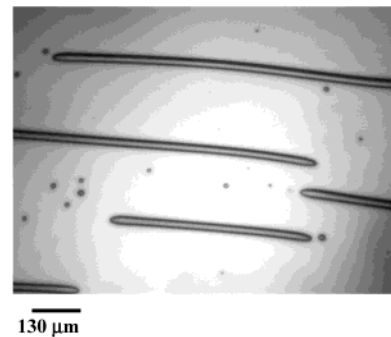


Figure 6. Optical micrograph of the morphology at $\dot{\gamma} = 3.0 \text{ s}^{-1}$.

At $\dot{\gamma} = 3.0 \text{ s}^{-1}$ ($\dot{\gamma}/\dot{\gamma}_d = 0.432$) the system also displays coexistence among droplets, squashed drops, and strings (see Figures 5 and 6). We focus our attention on strings in the discussion of Figures 5 and 6 due to their unique behavior, as we have already discussed the behavior of drops and squashed drops (cf. Figures 1–4). In Figure 5, where we plot a/d and b/d versus $2R_o/d$, we again see that the diameter of the strings has a narrow distribution (also evident in the micrograph in Figure 6) and is statistically independent of $2R_o/d$. A trivial consequence of the fact that b/d is almost independent of $2R_o/d$ is that the length of the strings in the flow direction becomes a *very strong* function of Ca .

$$(a/d) \propto (R_o/d)^{2.93 \pm 0.2}; \quad (b/d) \propto (R_o/d)^{0.03 \pm 0.02} \quad (9)$$

$$D \propto Ca^{2.93 \pm 0.2} \quad (10)$$

We had previously reported the formation of strings in confined emulsions,²⁷ and we can now identify another characteristic of a string by invoking the scaling of D with Ca . A string is characterized by the scaling relationship shown in eq 10. Taylor droplets certainly do not satisfy this scaling, while squashed droplets show a weaker dependence of a/b on Ca , and so this strong dependence of a/b on Ca is *unique* to strings in confined emulsions. *Isolated droplets (whose viscosities are matched with the matrix) when deformed so that Ca approaches 1 (or for whom D is $O(100)$, as seen in Figure 5) can only be transients in emulsions in bulk flows.* The stabilization provided by a combination of wall effects and the flow

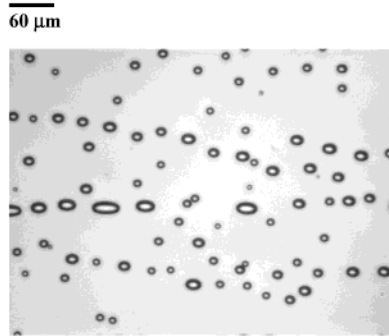


Figure 7. Optical micrograph of the morphology at $\dot{\gamma} = 6.5 \text{ s}^{-1}$.

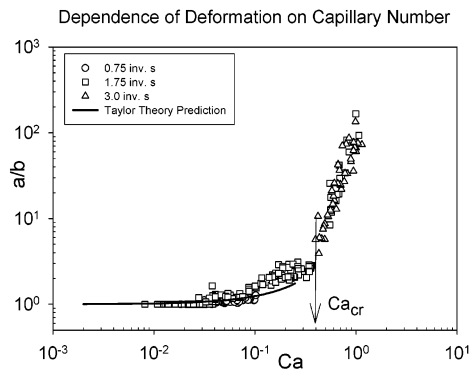


Figure 8. Droplet/string aspect ratio at different shear rates, plotted as a function of Capillary number. All points denote experimental data, while the Taylor theory prediction of the aspect ratio (continuous curve) and the single-droplet Ca_{cr} are also shown on the plot.

field²⁹ enables confined droplets to achieve extraordinarily large values of D . We have thus quantitatively demonstrated a critical difference between droplet deformation in the bulk and under confinement.

The effect of increasing shear on the strings is to elongate them while decreasing their radius. This is indeed observed as the shear rate is progressively increased from $\dot{\gamma} = 3.0 \text{ s}^{-1}$. The strings persist only until their diameter is at least half the gap width.^{29,33} We have already reported preliminary results on stability-related experiments (done with nearly the same experimental protocol as that for this study), and we consolidate those results here. Once the strings are sufficiently thin so that they no longer feel the stabilizing effect of the walls, they break up. In this state (and at all higher shear rates), droplets are recovered and are the only morphology observed in the system. Certainly, droplet/string breakup phenomena predominate under these conditions. This situation is depicted in Figure 7, where a micrograph at $\dot{\gamma} = 6.5 \text{ s}^{-1}$ ($\dot{\gamma}/\dot{\gamma}_d = 0.936$) is shown. These droplets are fairly small, certainly smaller than the gap width. At this shear rate, the limiting $2R^*/d$ ($=0.85$) is less than 1, which means that the droplets reach critical conditions and then break up, without ever being able to grow to the size of the gap width. Consequently, strings will not form at this shear rate (and higher shear rates), and only droplets will be observed.

In Figure 8, deformation data at a few different shear rates are plotted as a function of Ca on the same plot. This plot reiterates the fact that analysis of droplet deformation must be done in the framework of Ca (and not $\dot{\gamma}$). The curve suggests that if a confined drop attained a size corresponding to $Ca = 1.0$ at $\dot{\gamma} = 0.75 \text{ s}^{-1}$, its deformation would be $O(100)$. The single-drop Ca_{cr} and the Taylor

(33) Son, Y.-G.; Martys, N. S.; Migler, K. B. *Macromolecules* **2003**, *36*, 5825–5833.

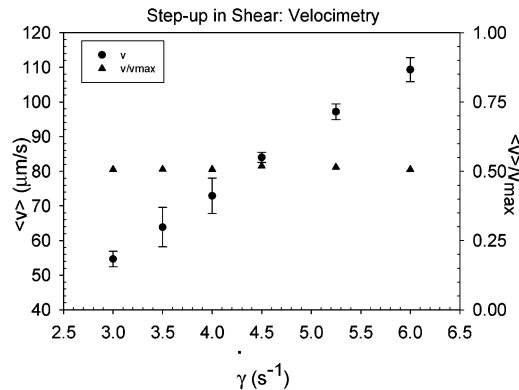


Figure 9. Average string velocity (dimensional form on left ordinate and dimensionless form on right ordinate) upon increase in shear. Bars on data points denote standard uncertainties equal to the standard deviation of the data.

theory prediction of a/b (vide eq 4) are also shown on the plot. For $Ca \leq 0.1$ (small droplets), Taylor theory does provide a reasonable estimate of a/b , in accord with our expectation. Taylor theory underpredicts the deformation associated with squashed droplets, whose deformation is enhanced by confinement. At larger Ca ($Ca > 0.1$), the a/b for the confined emulsion increases dramatically. We have already pointed out that this branch of the experimental deformation curve is *unique* to conditions of confinement. Any analytical theory for droplet deformation under confinement (no such theory exists to the best of our knowledge) would certainly have to predict this strong rise in deformation at supercritical Ca . Emulsions in shear flows in the bulk will certainly never show stretched nontransient droplets with $a/b O(100)$.

Why do strings disappear upon increase in shear rate, and what stabilizes them? To answer this question, we now discuss the data from a similar experiment²⁹ where the droplets were sheared at $\dot{\gamma} = 3 \text{ s}^{-1}$ for 10 h to form strings. The shear rate was then increased in small steps. We kept increasing the shear rate after the strings were formed, and at each shear rate we observed the response of the strings/droplets for 3 h, before increasing the shear rate to the next higher value. During the step up, the average string/droplet velocity $\langle v \rangle$ (determined by velocimetry) increases, as expected (see Figure 9). When the string velocity is divided by the velocity v_{max} ($=\dot{\gamma}d$) of the rotating plate, we find that v/v_{max} equals 0.5 within experimental error, at each new shear rate, suggesting that the strings/droplets are centered on the center line between the parallel plates. In the starting state ($\dot{\gamma} = 3 \text{ s}^{-1}$), strings are most likely already centered between the plates because wall migration^{9,22,34–43} overcomes droplet collisions in the one layer state²⁸ prior to string formation. Droplet collisions are essentially arrested in the one layer

(34) Goldsmith, H. L.; Mason, S. G. *J. Colloid Sci.* **1962**, *17*, 448–476.

(35) Karnis, A.; Mason, S. G. *J. Colloid Interface Sci.* **1967**, *24*, 164–169.

(36) Schowalter, W. R.; Chaffey, C. E.; Brenner, H. *J. Colloid Interface Sci.* **1968**, *26*, 152–160.

(37) Chaffey, C. E.; Brenner, H.; Mason, S. G. *Rheol. Acta* **1965**, *4*, 64–72.

(38) Chaffey, C. E.; Brenner, H.; Mason, S. G. *Rheol. Acta* **1967**, *6*, 100.

(39) Chan, P. C.-H.; Leal, L. G. *Int. J. Multiphase Flow* **1981**, *7*, 83–99.

(40) Chan, P. C.-H.; Leal, L. G. *J. Fluid Mech.* **1979**, *92*, 131–170.

(41) Smart, J. R.; Leighton, D. T. *Phys. Fluids A* **1991**, *3*, 21–28.

(42) Uijttewaal, W. S. J.; Nijhof, E.-J.; Heethaar, R. M. *Phys. Fluids, A* **1993**, *5*, 819–825.

(43) Uijttewaal, W. S. J.; Nijhof, E.-J. *J. Fluid Mech.* **1995**, *302*, 45–63.

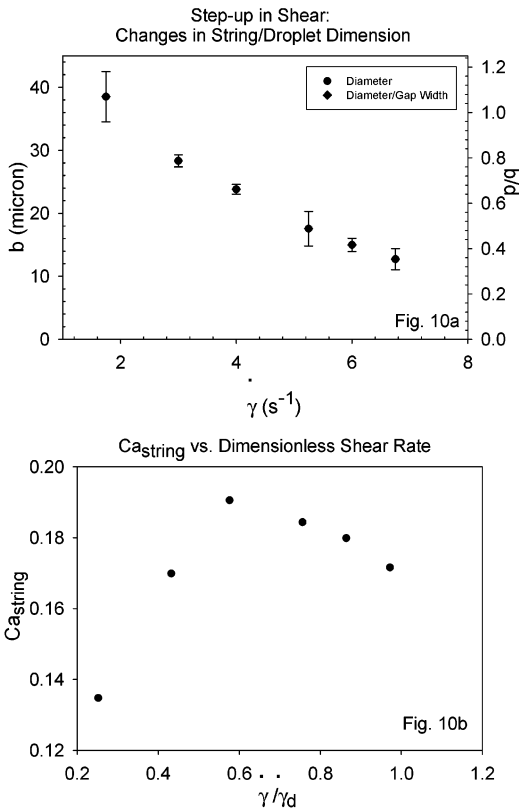


Figure 10. (a) Average string diameter in the vorticity direction (dimensional form on left ordinate and dimensionless form on right ordinate) upon increase in shear. Bars on data points denote standard uncertainties equal to the standard deviation of the data. (b) String Capillary number versus dimensionless shear rate.

state,²⁸ which the droplets first form at $\dot{\gamma} = 3 \text{ s}^{-1}$, followed by pearl necklace like arrangement of droplets and ultimately by coalescence to form strings.

Due to the increase in shear rate, the strings are elongated in the flow direction, accompanied by contraction in the velocity gradient and vorticity directions, to satisfy volume conservation constraints. We measured the droplet/string diameter in the vorticity direction (b) at various different shear rates (see Figure 10a). For the purpose of this discussion, it is assumed that the strings/droplets are axisymmetric, implying that the diameters in the velocity gradient and vorticity directions are equal. This assumption is legitimate in the direction of increasing shear, as the strengthening flow field progressively thins the strings/droplets, and the hydrodynamic interactions with the walls become weaker. Of course, this assumption fails when the walls squash the strings/droplets. The data in Figure 10a very clearly show that the string diameter is a function of shear rate, with strings becoming thinner upon increasing shear. Since it has been shown that droplet diameter does not control the string thickness (cf. Figure 5), what controls the string diameter? From dimensional analysis arguments, we infer that b/d is most likely a function of $\dot{\gamma}/\dot{\gamma}_d$. This result is suggested by these data (at a fixed gap width of $36 \mu\text{m}$) but can only be verified upon measurements of b for various different values of d .

Wall-induced stabilization is necessary but not sufficient for string stability. Even when the strings are wall-stabilized, flow is also necessary to keep them intact. When flow is turned off completely, well-known interfacial tension driven instabilities such as Rayleigh–Taylor–

Tomotika^{44–48} and end-pinch^{16,17} instabilities eventually break up the strings into droplets.²⁹ Simultaneous observation of morphology and measurement of string dimensions in the shear flow field offer insight into the physics behind string stability in the shear flow field. Strings persist with increasing shear until the diameter in the vorticity direction decreases to about half the gap width (note that some isolated droplets, which show little proclivity toward coalescence, are certainly present in the string regime, and they are ignored). When the shear rate is increased further, the strings become thinner, start to lose the stabilizing effects from the walls, and then break up. The breakup process is facilitated by string–drop and string–string interactions. At $\dot{\gamma} = 6.0 \text{ s}^{-1}$, the average diameter $b = 15 \mu\text{m}$, and breakup of strings becomes evident at this shear rate. As the shear rate is increased further, all the strings eventually break up into droplets. A plot of the string Capillary number,⁴⁹ $Ca_{\text{string}} = \eta_m(b/2)\dot{\gamma}/\sigma$, as a function of $\dot{\gamma}/\dot{\gamma}_d$ is shown in Figure 10b. We see that Ca_{string} first increases with increasing $\dot{\gamma}/\dot{\gamma}_d$ (in the strongly confined regime) and then decreases weakly with $\dot{\gamma}/\dot{\gamma}_d$, until a critical value of $Ca_{\text{cr,string}} = 0.184$ is reached at $\dot{\gamma} = 5.25 \text{ s}^{-1}$ ($b = 17.5 \mu\text{m}$). Stable strings with a smaller value of Ca_{string} than 0.184 are not observed upon further increase in $\dot{\gamma}$ (for $\dot{\gamma} > 5.25 \text{ s}^{-1}$).

Frischknecht⁴⁹ theoretically considered the stabilizing effect of shear on *infinitely long strings* in the *bulk* (no confinement effects) by performing a linear stability analysis on the coupled solutions to the Stokes and Cahn–Hilliard equations. She predicted that in order for a string to remain stable in a shear-flow field, Ca_{string} must exceed a certain critical value, $Ca_{\text{cr,string}}$. In other words, a weakly stretched string (larger diameter) is more stable than a strongly stretched string (smaller diameter). Note that this condition is *opposite* to that for the stability of a droplet, where stability is seen at subcritical Ca . She determined that, for $p = 1$, $Ca_{\text{cr,string}} = 0.18$, which is close to the value we determine for $Ca_{\text{cr,string}}$. At $\dot{\gamma} = 6.0 \text{ s}^{-1}$, where $b = 15 \mu\text{m}$, the stabilizing effects of the walls become weaker and the situation is somewhat closer to the bulk case ($b/d = 0.416$). Our finding that strings are unstable under these conditions is qualitatively consistent with the theoretical prediction of Frischknecht, who has noted that if a “long cylindrical drop” were considered instead of an infinite cylinder, small Brownian disturbances would indeed be suppressed by the flow, but as the drop thinned out to a critical radius, the disturbances would grow in amplitude, leading to its ultimate breakup. However, this finding should not be interpreted as a rigorous validation of the model, as the experiments involve finite-length strings that are indeed rather confined, signifying experimental conditions quite different from the assumptions built into the model.

Previously,²⁷ string stability was found for some (but not all) strings in a more concentrated mixture (28% PDMS/PIB) upon step-up in shear from low to high shear rates. We argue that it is likely that some of those strings were stable because they were sufficiently long to close off into closed rings, whose diameter obviously does not decrease with an increase in shear rate. Then Ca_{string} would increase with increasing shear, leading to enhanced stability, an effect predicted by the Frischknecht model.

(44) Lord Rayleigh. *Philos. Mag.* **1892**, *34*, 145–154.

(45) Lord Rayleigh. *Proc. London Math. Soc.* **1878**, *10*, 4–13.

(46) Chandrasekhar, S. *Hydrodynamic and Hydromagnetic Instability*; Clarendon Press: Oxford, 1961.

(47) Tomotika, S. *Proc. R. Soc. London, A* **1935**, *150*, 322–337.

(48) Tomotika, S. *Proc. R. Soc. London, A* **1936**, *153*, 302–318.

(49) Frischknecht, A. *Phys. Rev. E* **1998**, *58*, 3495–3514.

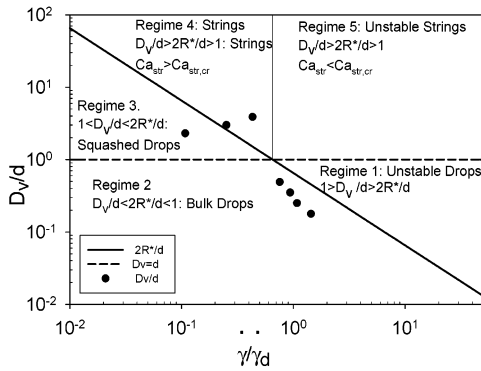


Figure 11. Regimes of string/droplet deformation in the parameter space of dimensionless size and dimensionless shear rate (for a system with a viscosity ratio of unity). Data points denote the experimentally determined volume average droplet diameter plotted versus dimensionless shear rate. The dimensionless gap width (constant) and dimensionless critical Taylor drop size are also shown on the plot as the dashed and continuous lines, respectively.

There is clearly a need for an analytical theory for thread breakup in the regime of finite-size effects. Newtonian thread breakup in a confined geometry (thread centered coaxially in a tube filled with another Newtonian fluid) has been treated by lattice–Boltzmann (LB) simulations.⁵⁰ We are in the process of extending the LB treatment along with complementary experimental measurements to multiple interacting threads confined between parallel platens.⁵¹

What morphology is associated with the greatest mass of the suspended phase at different shear rates? To answer this question and summarize our findings, we discuss the regimes of string/droplet behavior in the parameter space of dimensionless shear rate and dimensionless size. We describe the behavior of the volume average droplet diameter, D_v , determined by the coalescence and breakup behavior of the emulsion. We calculated $D_v = \sum_i n_i d_i^4 / \sum_i n_i d_i^3$ on the basis of the determined D_0 ($=2R_0$) values. The calculated nondimensional droplet sizes (normalized by d) are plotted versus dimensionless shear rate as the experimental data points in Figure 11. Also drawn on this plot are the Taylor prediction of $2R^*/d$ (vide eq 6) and the line where $D_v = d$.

We can divide this D_v versus $\dot{\gamma}$ parameter space into five regimes. Regime 1 corresponds to the case where the droplet Capillary number exceeds its critical value and the droplet diameter is less than the gap width. This corresponds to the familiar bulk case where the droplets are unstable; they elongate and break up. These two conditions are concisely expressed as follows.

$$\frac{2R^*}{d} < \frac{D_v}{d} < 1 \quad (11)$$

Naturally, we do not observe droplets in this “forbidden” regime, since they are unstable.

Regime 2 corresponds to the simple case of stable bulk droplets. This regime corresponds to subcritical droplet Capillary numbers (as usual), but an added constraint requires that the gap width exceed the droplet diameter. Combining these two constraints yields the following inequality.

$$\frac{D_v}{d} < \frac{2R^*}{d} < 1 \quad (12)$$

Even with small gaps on the order of tens of microns, the bulk behavior of emulsion droplets can indeed be recovered. This regime is seen at the low Capillary numbers in Figures 1 and 3.

Regime 3 corresponds to subcritical droplet Capillary numbers, but the droplet diameter *exceeds* the gap width. The observed morphology is the squashed droplet, as seen in Figures 3 and 4. It is defined by the following simultaneous inequalities.

$$1 < \frac{D_v}{d} < \frac{2R^*}{d} \quad (13)$$

The data show that the string regime (regime 4) corresponds to the case where the droplet Capillary number (defined in terms of the unperturbed equivalent droplet radius) is supercritical, while the equivalent droplet diameter exceeds the gap width. However, as the shear rate is increased beyond a critical value (cf. Figure 10), the strings become unstable and break up. This sets a third condition for the stability of the strings.

$$\frac{D_v}{d} > \frac{2R^*}{d} > 1$$

$$Ca_{\text{string}} > Ca_{\text{cr,string}} \quad (14)$$

The inequalities in eq 14 may be added to the “definition” of a string expressed earlier in this paper (cf. eq 10), along with the geometrical conditions that $a \gg d$ and $0.5d < b < d$ for a string.

The final regime (regime 5) corresponds to unstable strings, as seen in Figure 11, when the diameter of the string is less than a critical value. This regime is defined by the following conditions.

$$\frac{D_v}{d} > \frac{2R^*}{d} > 1$$

$$Ca_{\text{string}} < Ca_{\text{cr,string}} \quad (15)$$

Regimes 1 and 5 correspond to unstable droplets and strings, respectively. While we have used the line $D_v = d$ to demarcate the boundary between these regimes, the actual boundary between them is not completely clear at this point.

It is also interesting to observe the overall kinetics of coalescence and breakup as an emulsion is taken over a particular deformation history. In our experiments, we presheared at a high shear rate, $\dot{\gamma}/\dot{\gamma}_d = 1.44$, dropped the shear to the value of $\dot{\gamma}/\dot{\gamma}_d = 0.108$, and then used small increments in shear rate. The starting point of the deformation protocol, at $\dot{\gamma}/\dot{\gamma}_d = 0.108$, corresponds to droplets whose diameter is much smaller than the gap width. At the end of 3 h, coalescence had occurred, the corresponding D_v exceeded d , and squashed droplets were observed. Nevertheless, the system is frustrated by slow coalescence at this low shear rate, to allow the largest droplets to form strings. Therefore, the experimental data point at $\dot{\gamma}/\dot{\gamma}_d = 0.108$ lies in regime 3 and not in regime 4. As the shear rate is increased further, the increase in flow-driven coalescence causes droplets to become large enough to form strings. This explains why we have the unusual result that the droplet size increases with an increase in shear rate, due to very slow coalescence at

(50) Hagedorn, J. G.; Martys, N. S.; Douglas, J. F. *Phys. Rev. E*, submitted.

(51) Pathak, J. A.; Douglas, J. F.; Martys, N. S.; Hagedorn, J. G.; Migler, K. B. *Phys. Fluids*, to be submitted.

these low shear rates, making the time taken by the volume average diameter to attain its true steady-state value much longer than the time scale of the experiment. This phenomenon has been interpreted as a “hysteresis”⁵² between the breakup and coalescence curves in emulsions in bulk conditions. This “hysteresis” has been shown to be caused by the slow kinetics of coalescence and can be eliminated by shearing the mixture for longer times.⁵³ In the bulk, coalescence is likely slow, probably because of sufficiently large drop sizes that prevent film-drainage. However, under confinement the collision rate is smaller than that for the bulk,²⁸ leading to slower coalescence.⁵⁴

Conclusions

In summary, we have experimentally investigated the effect of microscopic confinement on droplet deformation in a system with a viscosity ratio of unity. We had shown earlier that confinement leads to formation of strings with remarkably large aspect ratios in these microconfined emulsions. Under conditions of flow, these string entities are very stable so long as they are not stretched too much

(52) Minale, M.; Mewis, J.; Moldenaers, P. *AIChE J.* **1998**, *44*, 943–950.

(53) Ramic, A. J.; Hudson, S. D.; Jamieson, A. M.; Manas-Zloczower, I. *Polymer* **2000**, *41*, 6263–6270.

(54) Loewenberg, M.; Hinch, E. J. *J. Fluid Mech.* **1997**, *338*, 299–315.

(55) Certain commercial materials and equipment are identified in this paper in order to adequately specify the experimental procedure. In no case does such identification imply recommendation or endorsement by the National Institute of Standards and Technology, nor does it imply that these are necessarily the best available for the purpose.

by the flow and continue to feel the stabilizing influence of the walls around them. Certainly, bulk deformation of droplets in an emulsion will never yield *stable* droplets with aspect ratios as large as those seen in this study—those droplets would undoubtedly be transients. This is a striking difference between droplet deformation in bulk and confined emulsions. We have therefore argued that confinement leads to enhanced droplet deformation and suppresses droplet breakup. Confinement also allows a larger stable “droplet” to exist, than what is predicted by the critical Capillary number. On the basis of the scaling for the dependence of the end-to-end length of a string on the equivalent drop radius, we have proposed a metric to “define” a string. This scaling also helps distinguish a string from morphologies such as small (weakly deformed) droplets and squashed droplets. We have identified the relevant length scales that are determinants of droplet deformation and microstructure and have divided the experimental droplet size versus shear rate parameter space into five regimes. In addition to the usual two bulk regimes (stable droplets and unstable droplets), we find three more regimes: two that correspond to confinement and one that corresponds to unstable strings.

Acknowledgment. We thank Prof. Alex Jamieson (Case Western Reserve University) for a loan of the shear cell. We also thank Steve Hudson and Jack Douglas (NIST) for helpful discussions, and we gratefully acknowledge numerous helpful comments by the reviewer.

LA0346907